

UC Irvine

UC Irvine Previously Published Works

Title

ENSO indices from sea surface salinity observed by Aquarius and Argo

Permalink

<https://escholarship.org/uc/item/5t12h1pr>

Journal

Journal of Oceanography, 70(4)

ISSN

0916-8370

Authors

Qu, Tangdong

Yu, Jin-Yi

Publication Date

2014-08-01

DOI

10.1007/s10872-014-0238-4

Copyright Information

This work is made available under the terms of a Creative Commons Attribution License, available at <https://creativecommons.org/licenses/by/4.0/>

Peer reviewed

ENSO indices from sea surface salinity observed by Aquarius and Argo

Tangdong Qu · Jin-Yi Yu

Received: 15 February 2014/Revised: 16 May 2014/Accepted: 17 May 2014/Published online: 4 June 2014
© The Oceanographic Society of Japan and Springer Japan 2014

Abstract Analysis of the first 26 months of data from the Aquarius satellite confirms the existence of a sharp sea surface salinity (SSS) front along the equator in the western equatorial Pacific. Following several earlier studies, we use the longitudinal location of the 34.8-psu isohaline as an index, termed Niño-S34.8, to measure the zonal displacement of the SSS front and consequently the eastern edge of the western Pacific warm pool. The on-going collection of the Array for Real-time Geostrophic Oceanography (ARGO) program data shows high correlations between Niño-S34.8 and the existing indices of El Niño, suggesting its potential important role in ENSO evolution. Further analysis of the ARGO data reveals that SSS variability in the southeastern tropical Pacific is crucial to identify the type of El Niño. A new SSS index, termed the southeastern Pacific SSS index (SEPSI), is defined based on the SSS variability in the region (0°–10°S, 150°–90°W). The SEPSI is highly correlated with the El Niño Modoki index, as well as the Trans-Niño index, introduced by previous studies. It has large positive anomalies during central Pacific El Niño or El Niño Modoki events, as a result of enhanced zonal sea surface temperature gradients between the central and eastern tropical Pacific, and can be used to characterize the type of El Niño. The processes that possibly control these SSS indices are also discussed.

Keywords Sea surface salinity · ENSO indices · Equatorial Pacific · Argo data · Aquarius ocean salinity

1 Introduction

The El Niño and Southern Oscillation (ENSO), as one of the most prominent climate phenomena in the equatorial Pacific, has been extensively studied in the past decades (e.g., Suarez and Schopf 1988; Weisberg and Wang 1997; Jin 1997; Picaut et al. 1997). In the western half of the equatorial Pacific, ENSO is seen as a zonal displacement of the warm (>28 °C) pool, eastward during El Niño and westward during La Niña. Though not well defined in sea surface temperature (SST), the eastern edge of the western Pacific warm pool is characterized by a sharp sea surface salinity (SSS) front, which separates the fresh western Pacific water from relatively salty central Pacific water. The SSS gradient associated with this SSS front varies from year to year and can sometimes reach as large as 1 psu in 1° longitude (e.g., Kuroda and McPhaden 1993; Donguy 1994; Eldin et al. 1997; Delcroix 1998; Picaut et al. 2001; Delcroix and McPhaden 2002; Maes et al. 2004).

Based on available SSS data during 1973–1995, Delcroix (1998) introduced an index of El Niño using the longitudinal location of the SSS front (i.e., the 35-psu isohaline) along the equator. Similar findings were derived from different time periods of SSS (e.g., Delcroix and Picaut 1998; Picaut et al. 2001; Singh et al. 2011 and references therein). These SSS indices vary consistently with the existing indices of El Niño, including the atmospheric Southern Oscillation index (SOI) and the oceanic Niño-3, Niño-3.4, and Niño-4 SST indices (e.g., Rasmusson and Carpenter 1982; Trenberth 1997). Since SSS does not have

T. Qu (✉)
International Pacific Research Center, SOEST, University of
Hawaii at Manoa, 1680 East-West Road, Honolulu 96822, HI,
USA
e-mail: tangdong@hawaii.edu

J.-Y. Yu
Department of Earth System Science, University of California,
Irvine, CA, USA

a direct atmospheric feedback, the use of SSS indices is expected to give different perspectives to characterize ENSO.

However, our understanding of the SSS indices has been hampered by the lack of salinity data. Most previous studies noted above were based on observations from Voluntary Observing Ships, TAO/TRITON moorings, and individual field experiments. The horizontal resolution of these data was relatively sparse and unable to precisely resolve the SSS front along the equator in the western equatorial Pacific. The successful launch of the Aquarius satellite offers a unique opportunity (Lagerloef et al. 2008), which has never been possible by conventional observations, to monitor the SSS variability in the region (e.g., Qu et al. 2014). Also recently available are the in situ data collected from a global array of profiling floats that measure the temperature and salinity in the upper 2,000 m under the framework of the Array for Real-time Geostrophic Oceanography (ARGO) program. Here, we examine the zonal displacement of the SSS front along the equator in the western equatorial Pacific and its validity as an index of El Niño, using the first 26 months of Aquarius measurements combined with the on-going collection of the Argo data. As a complement to the existing indices, we also introduce a new SSS index representing the SSS variability in the southeastern tropical Pacific to document the flavor and diversity of El Niño.

2 Data description

The first validated, geographically gridded dataset from Aquarius was recently released by the Ocean Salinity Science Team (<http://podaac.jpl.nasa.gov/aquarius>). This dataset, called the Aquarius/SAC-D version 2.0 data, was based on measurements by three separate microwave radiometers that measure brightness temperature along an approximately 390-km-wide swath using three separate beams with elliptical footprints of dimension 76×94 , 84×120 , and 96×156 km. The three non-overlapping beams sample the ocean differently from one another geographically and with different incidence angles that affect the salinity retrieval algorithm. The retrieved SSS data were bias-adjusted and mapped to a $1^\circ \times 1^\circ$ grid on weekly and monthly time scales. The Aquarius mission requirement is that the global salinity root mean square error is no more than 0.2 psu on 150×150 km and monthly average. As yet, the version 2 dataset partially achieves this requirement. See Lagerloef et al. (2013) for more details. The smoothed weekly and monthly SSS data from all three beams for the period from August 2011 to September 2013 are used in the present analysis.

A large number of Argo floats have been deployed in the past decade, and more than 3,500 of them are currently profiling over the global ocean (<http://www.argo.ucsd.edu>). The Argo floats record temperature and salinity at a vertical resolution of 1–5 m in the upper ocean and somewhat coarser at depth (25 m as the standard). The measurements extend from a typical top level around 5 m to about 2,000 m depth. Based on these measurements, a temperature/salinity product of the global ocean was recently created at the Asian Pacific Data Research Center of the International Pacific Research Center, University of Hawaii. This product provides near-real time temperature/salinity maps at a spatial resolution of 1° every month. It has 26 (standard) levels in the upper 2,000 m and spans

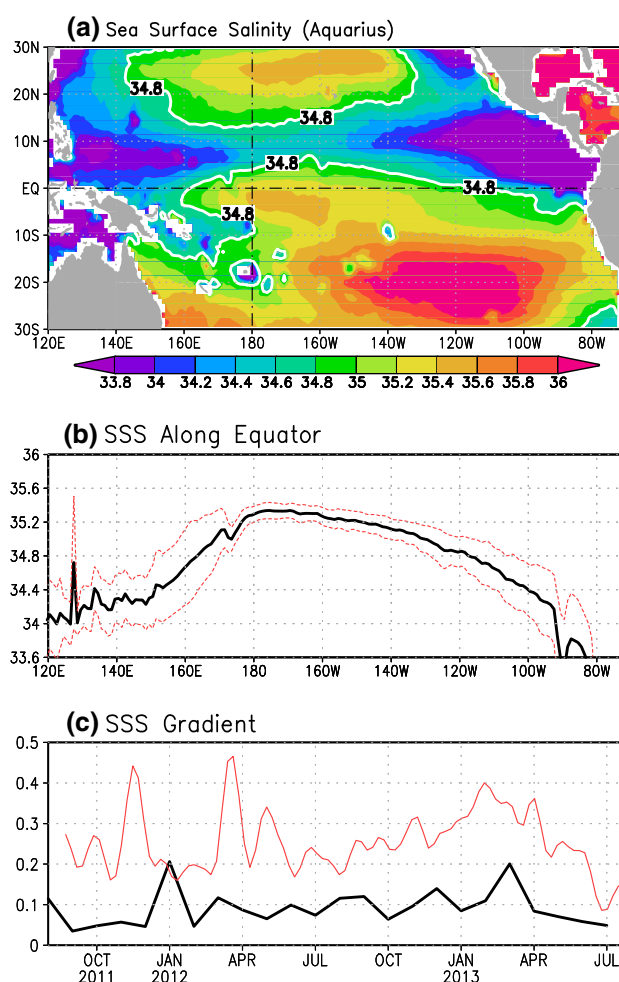


Fig. 1 Mean SSS (psu) **a** in the tropical Pacific and **b** along the equator (3°S – 3°N) from Aquarius during the period August 2011–September 2013. Also included **(c)** is the zonal SSS gradient (psu per degree longitude) across the 34.8-psu isohaline along the equator on monthly (*black*) and weekly (*red*) time scales, calculated using the grid points closest to the east and west sides of the 34.8 isohaline. The *black dot-dashed lines* in **(a)** indicate the equator and international dateline, respectively, and the *red light lines* in **(b)** show the range of one standard deviation above and below the mean values

from January 2005 to the present. In preparing this dataset, a variational analysis technique was used to interpolate temperature and salinity onto a three-dimensional spatial grid. For more details about this data product, see http://apdrc.soest.hawaii.edu/dods/public_data/Argo_Products/monthly_mean.

3 SSS front observed by Aquarius

During the period from August 2011 to September 2013, Aquarius captured most, if not all, of the SSS features in the Pacific (Fig. 1a), including the subtropical salinity maxima and the equatorial fresh water pools. Along the equator, a strong SSS front is detected west of the dateline, with a mean SSS of about 34.8 psu (Fig. 1b). Averaged over the period of observation, SSS increases from about 34.4 psu at 150°E to about 35.4 psu near the dateline, suggesting a mean SSS gradient of about 0.03 psu per degree longitude. This mean SSS gradient is significantly weaker than those from synoptic observations (e.g., Kuroda and McPhaden 1993; Donguy 1994; Eldin et al. 1997; Rodier et al. 2000; Maes et al. 2004; Maes 2008).

The SSS along the equator varies both in space and time (Fig. 1b). Its largest temporal variability occurs between about 150°E and the dateline, where its standard deviation (STD) or root mean square variation reaches 0.4 psu on monthly time scale. Large temporal variability is also seen

in the far western equatorial Pacific. This large variability may reflect the strong influence of land and coastal processes, as well as the inability of Aquarius to correctly sample the surface salinity near continental boundaries, both of which are beyond the scope of the present study.

Figure 1c shows the zonal SSS gradient across the 34.8-psu isohaline along the equator. The location of this isohaline is nearly identical with the location of the SSS front or the maximum zonal SSS gradient along the equator (Fig. 2a, b). On monthly average, the SSS gradient across the 34.8-psu isohaline is about 0.1 psu per degree longitude, but can occasionally reach 0.2 psu per degree longitude, larger than that derived from the annual mean SSS field by a factor at least 5. The SSS gradient is further enhanced by the use of weekly data, showing better agreement with synoptic observations (e.g., Kuroda and McPhaden 1993; Donguy 1994; Eldin et al. 1997; Maes et al. 2004). This result suggests that Aquarius, with a typical root mean square error of 0.2 psu on 150 × 150 km and monthly average (Lagerloef et al. 2013), is able to resolve the SSS front along the equator in the western equatorial Pacific.

The SSS front moves back and forth along the equator on various time scales (e.g., Delcroix 1998; Delcroix and Picaut 1998; Maes et al. 2004). Based on the monthly data from space, Qu et al. 2014 recently reported that Aquarius can precisely detect the zonal displacement of the SSS front (their fig. 6). Using the 34.8-psu isohaline as a proxy,

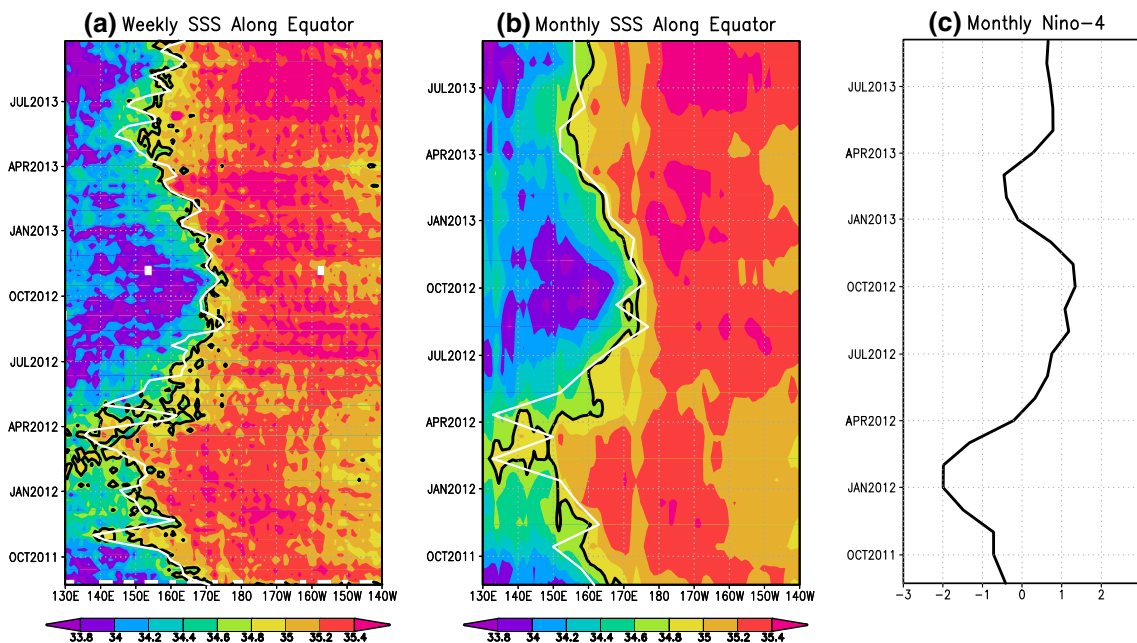


Fig. 2 SSS (psu) along the equator (3°S–3°N) on **a** weekly and **b** monthly time scales from Aquarius, compared with **c** the Niño-4 index from Argo normalized by its standard deviation during the period August 2011–September 2013. The *black contours* in (a,

b) indicate the 34.8-psu isohaline, and the white contours show the location of maximum zonal SSS gradient in the range between 34.4 and 35.3 psu

they noted that the SSS front detected by Aquarius migrates over a longitude band larger than 40° , and its zonal displacement is rather consistent with that observed by Argo. Despite some differences in small scale structures, the weekly Aquarius data (Fig. 2a) show essentially the same variability as the monthly data (Fig. 2b). During the 2011/12 La Niña event, the SSS front moved westward to as far as 140°E from its mean location near 163°E . For the period from August 2011 to September 2013, the SSS front detected by Aquarius is highly correlated with the Niño-4 index (Fig. 2c) derived from the Argo SST (discussed in Sect. 4), and their correlation coefficient reaches 0.72, with the latter leading by about 2 months.

4 Indices of El Niño

The newly available Aquarius and Argo data enable us to examine the SSS indices of El Niño in more detail. The first index, termed Niño-S34.8 hereinafter, is defined as the longitudinal location of the 34.8-psu isohaline along the equator, representing the SSS front near the eastern edge of the western Pacific warm pool (Fig. 1). This definition differs only slightly from that by Delcroix (1998), who used the 35.0-psu isohaline as a proxy of the SSS front. Results from the Aquarius and Argo data confirm the correspondence between the SSS front and ENSO and that what has been discussed by previous studies (e.g., Delcroix 1998) based on relatively coarse resolution data is mostly valid.

To further demonstrate how the Niño-S34.8 index works, we examine the Argo product described in Sect. 2 and compare Niño-S34.8 with the SST indices of El Niño from Argo (Fig. 3a). Following the definition of Trenberth (1997) and Trenberth and Stepaniak (2001), we calculate the Niño-3, Niño-4, and Niño-3.4 indices as regional averages of SST at (5°S – 5°N , 150° – 90°W), (5°S – 5°N , 160°E – 150°W), and (5°S – 5°N , 170° – 120°W), respectively. The correspondence between the SSS front and ENSO has been reported by previous studies (e.g., Delcroix 1998; Picaut et al. 2001; Maes et al. 2004; Bosc et al. 2009; Singh et al. 2011; Qu et al. 2014). Here, we note that the correlation between the Niño-S34.8 and Niño-4 indices reached as high as 0.88 during the Argo period (January 2005–September 2013), with the latter leading by 1 month (Fig. 3a). The Niño-S34.8 index is also highly ($r = 0.75$) correlated with Niño-3.4, while its correlation with Niño-3 is somewhat lower ($r = 0.54$). On average, Niño-S34.8 lags Niño-3.4 and Niño-3 by 2–3 months, but, during the developing phase of El Niño events (e.g., 2006/07 and 2009/10), the opposite happens, indicating that El Niño starts from the western equatorial Pacific (Fig. 3a). No

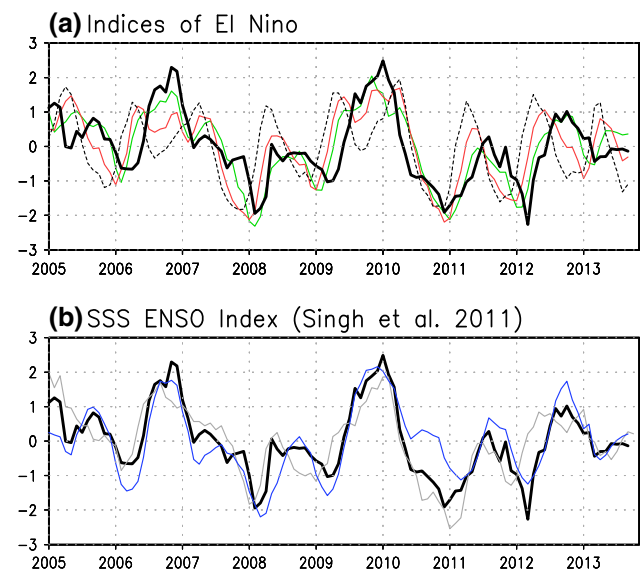


Fig. 3 Time series of **a** normalized Niño-S34.8 (thick black), Niño-4 (green), Niño-3.4 (red), and Niño-3 (black dashed) indices, and **b** normalized SOI (gray) and SSS ENSO index (blue) introduced by Singh et al. (2011) from Argo for the period January 2005–September 2013. The Niño-S34.8 index is averaged over the latitude band between 3°S and 3°N

similar phenomena can be found during the developing phase of La Niña.

Based on a gridded SSS product derived from observations of Voluntary Observing Ships, TAO/TRITON moorings, and Argo profilers, Singh et al. (2011) recently introduced an index called the SSS ENSO index, defined as the difference between the normalized SSS anomalies averaged in the regions (25° – 10°S , 160°E – 160°W) and (2°S – 2°N , 150°E – 170°W). For comparison, the SSS ENSO index calculated from the Argo data is shown in Fig. 3b. In general, the SSS ENSO index shows a good ($r = 0.83$) correspondence with Niño-S34.8. If lagging by 2 months, the correlation between the SSS ENSO index and SOI reaches -0.66 , which is slightly lower than that (-0.84) between the Niño-S34.8 index and SOI. This result suggests that both indices can be used to characterize the salinity evolution during El Niño events. With their different definitions, the two indices may complement each other in understanding the ENSO dynamics.

To further illustrate the basin scale structure of El Niño, Fig. 4 shows the regression coefficients of SST and SSS toward the Niño-S34.8 index in the tropical Pacific. As one would expect, high regression coefficients (>0.06) of SST are seen along the equator (Fig. 4a), consistent with the typical SST anomaly pattern during El Niño events. The regression coefficients of SSS are dominated by a pattern that consists of one negative and three positive cores (Fig. 4b). The negative core roughly coincides with the

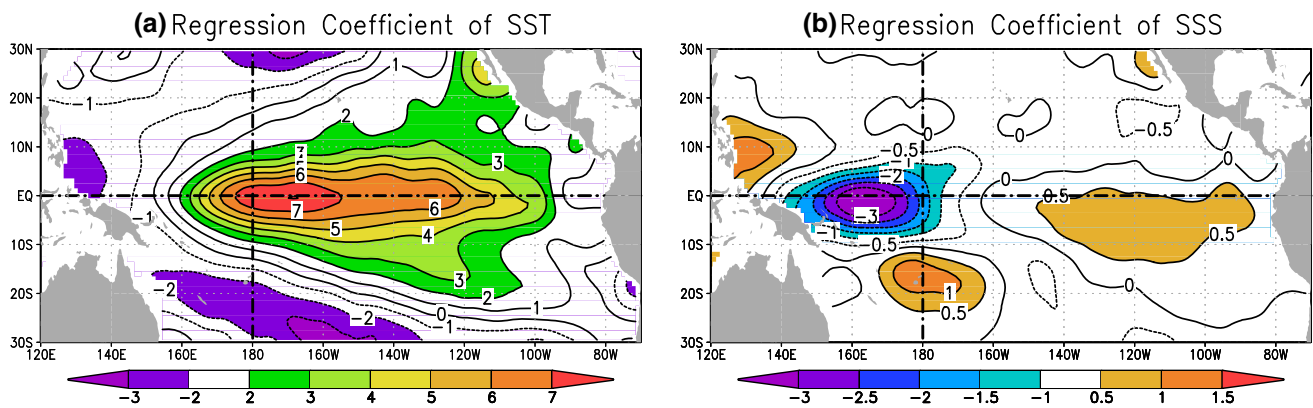


Fig. 4 Regression coefficients of **a** SST and **b** SSS toward the Niño-S34.8 index in the tropical Pacific for the period January 2005–September 2013. The mean seasonal cycles have been removed from

mean SSS front at about 163°E along the equator. The positive cores are found near the Philippine coast, over the South Pacific Convergence Zone (SPCZ), and in the southeastern tropical Pacific, respectively. The appearance of high SSS variability off the Philippines, as well as the contrasted SSS patterns in the equatorial part of the warm pool and along the mean SPCZ position, has been discussed by Delcroix (1998) (their plate 3b) and Singh et al. (2011) (their fig. 4). The broad positive regression coefficient of SSS in the southeastern tropical Pacific is a new feature identified here for El Niño. Though also visible in Singh et al.'s (2011) SSS map (their fig. 5b), it has not been explicitly discussed before. The SSS anomaly centers used to define the SSS ENSO index of Singh et al. (2011), for example, are all located in the western half of the tropical Pacific. The SSS anomalies in the southeastern tropical Pacific may reflect the influence of large-scale wind anomalies, which in turn are closely related to the zonal SST gradients between the central and eastern equatorial Pacific (discussed in Sect. 5). We therefore speculate that the SSS anomalies in the southeastern tropical Pacific are useful parameter characterizing the type of El Niño. The details are examined below.

Different types of El Niño have been identified by previous studies. Among others, Yu and Kao (2007) and Kao and Yu (2009) reported two types of El Niño in the tropical Pacific: an eastern Pacific type and a central Pacific type. The central Pacific El Niño was also termed “El Niño Modoki” by Ashok et al. (2007), as a tropical ocean–atmosphere-coupled phenomenon that may be distinct from the conventional eastern Pacific El Niño. Two examples of central Pacific El Niño are found in 2004/05 and 2009/10 (Ashok et al. 2007; Yu et al. 2012), with warming in the central tropical Pacific, flanked by cooler than normal or at least close to zero SST anomalies in the western and eastern Pacific.

the time series before calculation. The black dot-dashed lines indicate the equator and international dateline, respectively. Units are 10^{-2} °C per degree longitude in (a) and 10^{-2} psu per degree longitude in (b)

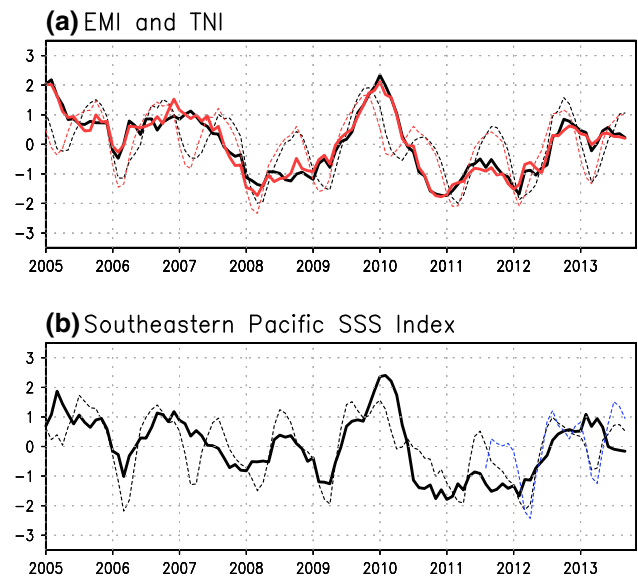


Fig. 5 **a** Time series (dashed line) of normalized ENSO Modoki index (EMI; black) as defined by Ashok et al. (2007) and Trans-Niño index (TNI; red) as defined by Trenberth and Stepaniak (2001). **b** Time series (dashed line) of normalized southeastern Pacific SSS index (SEPSI) introduced by the present study. The solid lines in both (a) and (b) indicate interannual variability relative to the mean seasonal cycle, and the blue dashed line in (b) shows the SEPSI from Aquarius

To better describe this phenomenon, Ashok et al. (2007) proposed an El Niño Modoki index (EMI), which represents the SST difference between the central tropical Pacific and the eastern and western parts of the basin. The EMI derived from Argo is shown in Fig. 5a. Also included in this figure is the Trans-Niño index (TNI) introduced by Trenberth and Stepaniak (2001), defined as the difference of normalized SST anomalies between the Niño-4 and Niño-1 + 2 regions. As already noted by several earlier studies (e.g., Ashok et al. 2007; Takahashi et al. 2011), the two indices are almost identical, with their correlation

exceeding 0.92 for the period of observation. Two peaks stand out in both time series, corresponding to the central Pacific El Niño or El Niño Modoki events in 2004/05 and 2009/10, respectively. Both indices have positive anomalies of more than two standard deviations during central Pacific El Niño, while their anomalies during eastern Pacific El Niño (e.g., 2006/07) are relatively small (Fig. 5a).

Since the EMI and TNI indices represent the large-scale zonal SST gradients along the equator, it seems to be a natural idea that SSS must respond to variations of these SST indices through both atmospheric and oceanic processes. It is noticed that the regression coefficient of SST toward the Niño-S34.8 index approaches its maximum (~ 0.06) near the dateline on the equator (see Fig. 4a). Relatively high values (~ 0.04) also extend northeastward toward Baja California, which is similar to the SST anomaly pattern of the central Pacific El Niño or El Niño Modoki (e.g., Weng et al. 2007; Kao and Yu 2009). To some extent, this correlation pattern reflects the fact that two of the three El Niño events included in the analysis period are the central Pacific type of El Niño. As a consequence, the SSS regression pattern shown in Fig. 4b must also reflect the SSS characteristics of the central Pacific El Niño. We notice that, among the four cores of the regression pattern, only the positive core in the southeastern tropical Pacific does not appear in the SSS anomaly pattern associated with the eastern Pacific El Niño obtained by Singh et al. (2011) (see their fig. 4). Having this idea in mind, we introduce a new index called southeastern Pacific SSS index (SEPSI) as the regional average of SSS at (0° – 10° S, 150° – 90° W). The region selected roughly coincides with the positive core of the SSS regression anomalies pattern (Fig. 4b).

The SEPSI index (Fig. 5b) was positive during all El Niño events (e.g., 2004/05, 2006/07, and 2009/10), but it peaked only in 2004/05 and 2009/10, when a central Pacific El Niño took place. The overall correlation between the SEPSI and EMI/TNI reached 0.84 for the period from January 2005 to September 2013. The SEPSI from Aquarius was also highly ($r = 0.85$) correlated with the EMI/TNI indices (Fig. 5b). With this new index and the above-introduced Niño-S34.8 index, SSS can be used to characterize El Niño event and type. When Niño-S34.8 has a positive anomaly larger than its threshold value (e.g., two standard deviations), one can anticipate that an El Niño is taking place. Then, if the SEPSI anomaly exceeds its threshold value, the event is most likely a central Pacific El Niño.

It is worth noting that we have also calculated the SSS El Niño index introduced by Singh et al. (2011), defined as the normalized difference between the normalized SSS anomalies averaged in regions B (2° S– 2° N, 170° E– 170° W)

and A (2° S– 2° N, 150° – 170° E). They defined this index to identify the type of El Niño. For the Argo period, neither the correlation between the SSS El Niño index and SEPSI nor the correlation between the SSS El Niño index and EMI/TNI is significant (data not shown). The causes of this low correlation are not yet understood. They could result in part from the shortness of the Argo data time series, or from the difference of definitions used by the two studies. In defining the SSS El Niño index, Singh et al. (2011) emphasize the importance of SSS gradient between the central and western Pacific, while the present study focuses on the regional average of SSS anomalies in the southeastern tropical Pacific. The two indices emphasize different aspects of salinity anomalies during central Pacific El Niño or El Niño Modoki events and require further investigations to understand their differences.

5 Forcing processes

To examine the processes that possibly control the SSS indices, Fig. 6 shows the SST, SSS, precipitation minus evaporation (P–E), and wind stress anomalies during the mature phase (December–February) of the 2006/07 and 2009/10 El Niño events relative to their respective mean seasonal cycles. As one would expect, the western Pacific warm pool shifted eastward when the 2009/10 El Niño started to occur (Fig. 6a). By the end of 2009, the 29° C isotherm has reached about 160° W, where SST anomalies exceeded 2° C. In contrast, the SST anomalies in the far eastern tropical Pacific were small and even negative south of the equator, suggesting anomalous SST gradients in the zonal direction. These anomalous SST gradients further generated northwestward wind anomalies, helping maintain the maximum SST anomalies in the central equatorial Pacific near 160° W.

The eastward shift of the western Pacific warm pool was followed by an eastward displacement of the SSS front (Fig. 6b) and heavy rainfall (Fig. 6c). During the mature phase of the 2009/10 El Niño event, the SSS front as indicated by the 34.8-psu isohaline reached about 170° W. On the western side of the SSS front, negative SSS anomalies took place, with a maximum magnitude exceeding 0.7 psu near 170° E. On the eastern side of the SSS front, the SSS anomalies were generally positive, except for a narrow longitude band off the American coast. The P–E anomalies in the equatorial Pacific showed a consistent pattern with the SSS anomalies, except that their zero line was about 20° longitude farther eastward than that of SSS anomalies, reflecting strong influence of ocean processes (Fig. 6c). Of particular interest are the large, negative P–E anomalies (approximately -3 mm day $^{-1}$) lying between 140° W and 90° W within about 10° south of

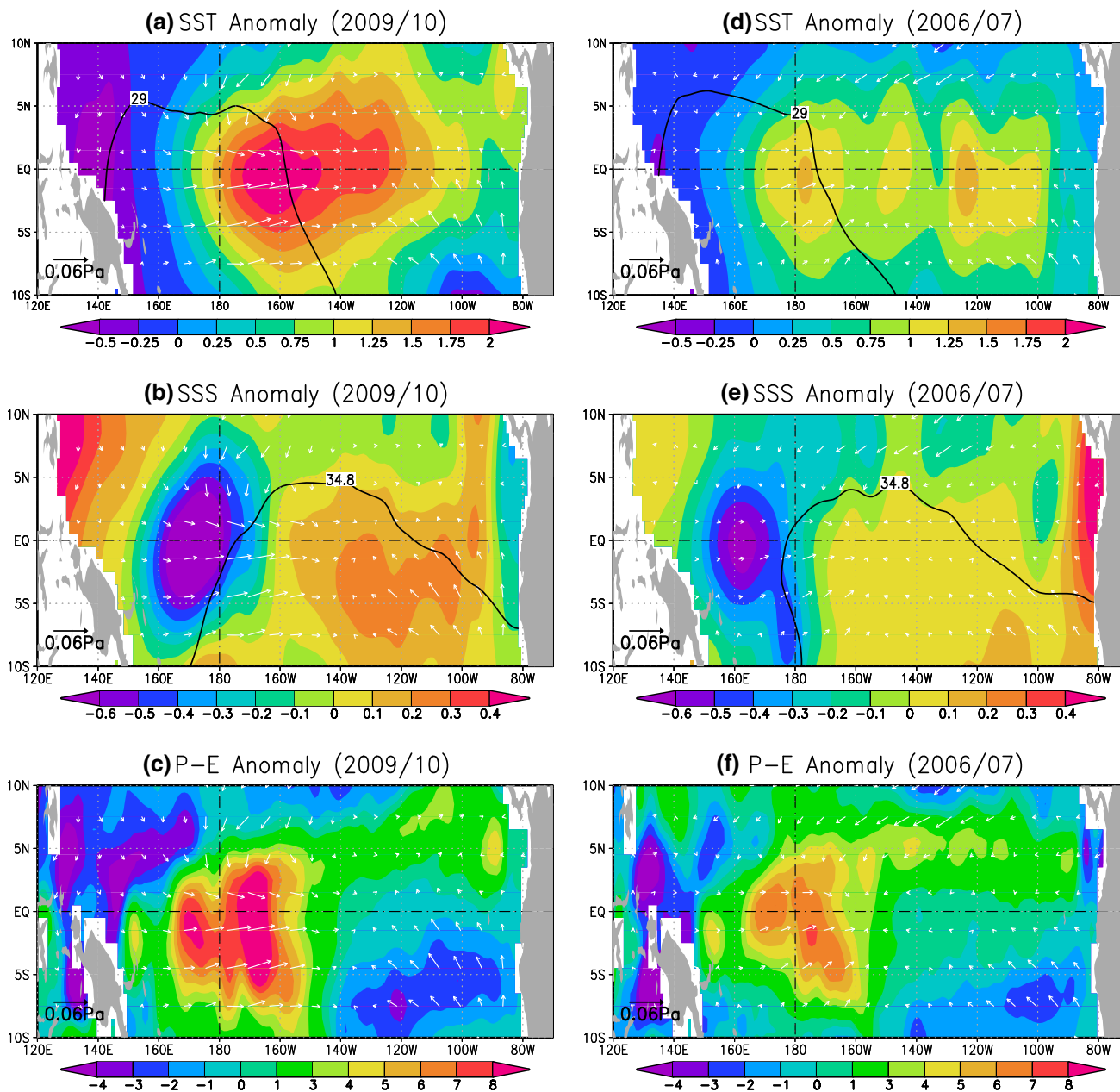


Fig. 6 Anomalous SST (*upper*) and SSS (*middle*) from Argo and P-E (*lower*) from the National Centers for Environmental Prediction (NCEP)/National Center for Atmospheric Research (NCAR) Re-analysis Project (Kalnay et al. 1996) during December 2009–February 2010 (a–c) and December 2006–February 2007 (d–f). *White vectors*

indicate anomalous wind stress, *black lines* represent the 29 °C isotherm and 34.8-psu isohaline, and the *black dot-dashed lines* indicate the equator and international dateline. Units are °C for SST, psu for SSS, mm day⁻¹ for P-E, and N m⁻² or Pa for wind stress

the equator, presumably as a consequence of enhanced northwestward wind anomalies forced by anomalous SST gradients between the central and eastern equatorial Pacific (Fig. 6a). These negative P-E anomalies further generated positive SSS anomalies in the southeastern tropical Pacific (Fig. 6b), with a maximum exceeding 0.2 psu in the region where SEPSI was defined.

The SST anomalies during the 2006/07 El Niño event (Fig. 6d) were smaller and more widely spread than those during the 2009/10 event (Fig. 6a). The reduced zonal SST gradients along the equator generated weaker northwestward wind anomalies, which in turn induced weaker P-E (Fig. 6e) and SSS (Fig. 6f) anomalies in the southeastern tropical Pacific. We attribute these differences to the type

or location difference between the two events. However, given the fact that the 2006/07 El Niño is relatively weak, we cannot exclude the possibility that the intensity difference between the two events also plays a role.

6 Summary and discussion

The SSS front associated with the eastern edge of the western Pacific warm pool has been discussed by previous studies, and its link to ENSO has long been recognized (e.g., Delcroix 1998; Delcroix and Picaut 1998; Bosc et al. 2009; Singh et al. 2011; Qu et al. 2014). The present study, based on newly available satellite (Aquarius) and in situ (mainly Argo) observations, confirms the high correlation of the SSS front with ENSO. As a proxy of the SSS front, we define the longitudinal location of the 34.8-psu isohaline as an index of El Niño, termed Niño-S34.8, which is slightly different from those introduced by previous studies (e.g., Delcroix 1998; Bosc et al. 2009). This index is independent of the longitudinal location of El Niño, and is capable of identifying any types of El Niño, consistent with what has been discussed by Delcroix (1998) and Bosc et al. (2009). Another SSS index introduced by the present study is SEPSI representing regional average of SSS anomalies in the southeastern tropical Pacific. Differing from the SSS index defined by Singh et al. (2011), our index emphasizes the importance of a large-scale SSS gradient between the central and eastern equatorial Pacific. The SEPSI appears to be stronger during the central Pacific El Niño events than during the eastern Pacific El Niño events. A combined use of the Niño-S34.8 index and SEPSI enables us to identify ENSO events and their types. In addition, we note that a better understanding of the SSS variability in the southeastern tropical Pacific is crucial to the studies of ENSO diversity.

As a complement to the existing SST indices of El Niño, SSS indices may help reveal new characteristics of ENSO. For example, a negative feedback exists between the ocean's surface temperature and heat flux, but not between the ocean's surface salinity and freshwater flux. As such, the ocean's surface temperature and salinity are possibly governed by different processes. In particular, since the damping processes for salinity are oceanic and less efficient than those for temperature, SSS variability is expected to have more power than SST variability towards lower frequencies and can be traced in ocean circulation for years (e.g., Spall 1993; Mignot and Frankignoul 2004). In a similar way, the variability in SSS indices during an El Niño event can result from the variability in ocean circulation a few years or even a few decades back, suggesting some potential advantage of using SSS indices in

understanding the interannual to decadal variability of the equatorial Pacific.

As longer time series of Aquarius and Argo data become available, SSS indices, such as those defined in the present study, can be used to further understand the ocean processes that govern the El Niño variability on interannual to decadal time scales. Also available for future studies are the SSS data from the Soil Moisture and Ocean Salinity (SMOS) satellite (<https://earth.esa.int/web/guest/missions/esa-operational-eo-missions/smos>), as well as from other in situ platforms, including those collected from VOS, TAO/TRITON moorings, and individual field experiments. Based on these available in situ observations, Delcroix et al. (2011) have created a gridded SSS product of the global ocean for the period from 1950 to 2009. The combined use of this product with the on-going collection of satellite (i.e., Aquarius and SMOS) and Argo data will provide a unique opportunity to investigate the SSS indices and their role in ENSO evolution. We will leave this for future studies.

Acknowledgments T. Qu was supported by NASA as part of the Aquarius Science Team investigation through grant NNX12AG02G and by NSF through grant OCE11-30050. J.-Y. Yu was supported by NSF through grant AGS-1233542. The authors are grateful to N. Schneider, Y.T. Song, and C. Maes for many useful discussions on the topic and to T. Tozuka and three anonymous reviewers for the thoughtful comments and suggestions. School of Ocean and Earth Science and Technology contribution number 9123, and International Pacific Research Center contribution number IPRC-1058.

References

- Ashok K, Behera SK, Rao SA, Weng H, Yamagata T (2007) El Niño Modoki and its possible teleconnection. *J Geophys Res* 112:C11007. doi:10.1029/2006JC003798
- Bosc C, Delcroix T, Maes C (2009) Barrier layer variability in the western Pacific warm pool from 2000 to 2007. *J Geophys Res* 114:C06023. doi:10.1029/2008JC005187
- Delcroix T (1998) Observed surface oceanic and atmospheric variability in the tropical Pacific at seasonal and ENSO timescales: a tentative overview. *J Geophys Res* 103:18611–18633. doi:10.1029/98JC00814
- Delcroix T, Alory G, Cravatte S, Corrège T, McPhaden M (2011) A gridded sea surface salinity data set for the tropical Pacific with sample applications (1950–2008). *Deep Sea Res Part I* 58(1):38–48. doi:10.1016/j.dsr.2010.11.002
- Delcroix T, McPhaden MJ (2002) Interannual sea surface salinity and temperature changes in the western Pacific warm pool during 1992–2000. *J Geophys Res* 107:8002. doi:10.1029/2001JC000862
- Delcroix T, Picaut J (1998) Zonal displacement of the western equatorial Pacific “fresh pool”. *J Geophys Res* 103:1087–1098. doi:10.1029/97JC01912
- Donguy JR (1994) Surface and subsurface salinity in the tropical Pacific Ocean: relations with climate. *Prog Oceanogr* 34:45–78
- Eldin G, Rodier M, Radenac M-H (1997) Physical and nutrient variability in the upper equatorial Pacific associated with

- westerly wind forcing and wave activity in October 1994. *Deep Sea Res Part II* 44:1783–1800
- Jin FF (1997) An equatorial ocean recharge paradigm for ENSO. Part I: conceptual model. *J Atmos Sci* 54:811–829
- Kalnay E, Coauthors (1996) The NCEP/NCAR 40-year reanalysis project. *Bull Am Meteorol Soc* 77:437–371
- Kao H-Y, Yu J-Y (2009) Contrasting Eastern-Pacific and Central-Pacific types of ENSO. *J Clim* 22:615–632
- Kuroda Y, McPhaden MJ (1993) Variability in the western equatorial Pacific Ocean during JAPACS cruises in 1989 and 1990. *J Geophys Res* 98:4747–4759
- Lagerloef G, Coauthors (2013) Aquarius salinity validation analysis; data version 2.0. Aquarius project document, AQ-014-PS-0016, p 36
- Lagerloef G, Colomb FR, Le Vine D, Wentz F, Yueh S, Ruf C, Lilly J, Gunn J, Chao Y, deCharon A, Feldman G, Swift C (2008) The Aquarius/SAC-D mission: designed to meet the salinity remote-sensing challenge. *Oceanography* 21:68–81
- Maes C (2008) On the ocean salinity stratification observed at the eastern edge of the equatorial Pacific warm pool. *J Geophys Res* 113:C03027. doi:10.1029/2007JC004297
- Maes C, Picaut J, Kuroda Y, Ando K (2004) Characteristics of the convergence zone at the eastern edge of the Pacific warm pool. *Geophys Res Lett* 31:L11304. doi:10.1029/2004GL019867
- Mignot J, Frankignoul C (2004) Interannual to interdecadal variability of sea surface salinity in the Atlantic and its link to the atmosphere in a coupled model. *J Geophys Res* 109(C04005):14. doi:10.1029/2003JC002005
- Picaut J, Masia F, du Penhoat Y (1997) An advective–reflective conceptual model for the oscillatory nature of the ENSO. *Science* 277:663–666
- Picaut J, Ioualalen M, Delcroix T, Masia F, Murtugudde R, Vialard J (2001) The oceanic zone of convergence on the eastern edge of the Pacific warm pool: a synthesis of results and implications for El Niño Southern Oscillation and biogeochemical phenomena. *J Geophys Res* 106:2363–2386. doi:10.1029/2000JC900141
- Qu T, Song YT, Maes C (2014) Sea surface salinity and barrier layer variability in the equatorial Pacific as seen from Aquarius and Argo. *J Geophys Res* 119. doi:10.1002/2013JC009375
- Rasmusson EM, Carpenter TH (1982) Variations in tropical sea surface temperature and surface wind fields associated with the Southern Oscillation/El Niño. *Mon Weather Rev* 110:354–384. doi:10.1175/1520-0493(1982)110<0354:VITSST>2.0.CO;2
- Rodier M, Eldin G, Le Borgne R (2000) The western boundary of the equatorial Pacific upwelling: some consequences of climatic variability on hydrological and planktonic properties. *J Oceanogr* 56:463–471
- Singh A, Delcroix T, Cravatte S (2011) Contrasting the flavors of El Niño and Southern Oscillation using sea surface salinity observations. *J Geophys Res* 116:C06016. doi:10.1029/2010JC006862
- Spall MA (1993) Variability of sea surface salinity in stochastically forced systems. *Clim Dyn* 8:151–160
- Suarez MJ, Schopf PS (1988) A delayed oscillator for ENSO. *J Atmos Sci* 45:3283–3287
- Takahashi K, Montecinos A, Goubanova K, Dewitte B (2011) ENSO regimes: reinterpreting the canonical and Modoki El Niño. *Geophys Res Lett* 38:L10704. doi:10.1029/2011GL047364
- Trenberth KE (1997) The definition of El Niño. *Bull Am Meteorol Soc* 78(12):2771–2777. doi:10.1175/1520-0477(1997)078<2771:TDOENO>2.0.CO;2
- Trenberth K, Stepaniak DP (2001) Indices of El Niño evolution. *J Clim* 14:1697–1701
- Weisberg RH, Wang C (1997) A western Pacific oscillator paradigm for the El Niño–Southern Oscillation. *Geophys Res Lett* 24:779–782
- Weng H, Ashok K, Behera SK, Rao SA, Yamagata T (2007) Impacts of recent El Niño Modoki on droughts/floods in the Pacific Rim during boreal summer. *Clim Dyn* 29:113–129. doi:10.1007/s00382-007-0234-0
- Yu J-Y, Kao H-Y (2007) Decadal changes of ENSO persistence barrier in SST and ocean heat content indices: 1958–2001. *J Geophys Res* 112:D13106. doi:10.1029/2006JD007654
- Yu J-Y, Zou Y, Kim ST, Lee T (2012) The changing impact of El Niño on US winter temperatures. *Geophys Res Lett* 39:L15702. doi:10.1029/2012GL052483